ACS Synthetic Biology

pubs.acs.org/synthbio
Research Article

Functional Deimmunization of Botulinum Neurotoxin Protease Domain via Computationally Driven Library Design and Ultrahigh-Throughput Screening

Yongliang Fang,[#] Andrew Y. Chang,[#] Deeptak Verma, Shin-Ichiro Miyashita, Susan Eszterhas, Pyung-Gang Lee, Yi Shen, Lydia R. Davis, Min Dong, Chris Bailey-Kellogg, and Karl E. Griswold*

Cite This: *ACS Synth. Biol.* 2023, 12, 153−163

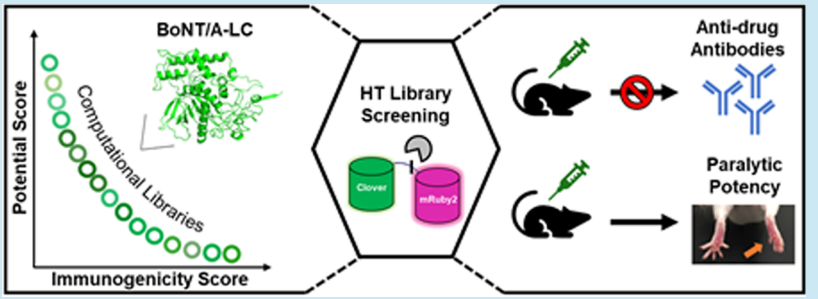

ABSTRACT: Botulinum neurotoxin serotype A (BoNT/A) is a widely used cosmetic agent that also has diverse therapeutic applications; however, adverse antidrug immune responses and associated loss of efficacy have been reported in clinical uses. Here, we describe computational design and ultrahigh-throughput screening of a massive BoNT/A light-chain (BoNT/A-LC) library optimized for reduced T cell epitope content and thereby dampened immunogenicity. We developed a functional assay based on bacterial co-expression of BoNT/A-LC library members with a Förster resonance energy transfer (FRET) sensor for BoNT/A-LC enzymatic activity, and we employed high-speed fluorescence-activated cell sorting (FACS) to identify numerous computationally designed variants having wild-type-like enzyme kinetics. Many of these variants exhibited decreased immunogenicity in humanized HLA transgenic mice and manifested *in vivo* paralytic activity when incorporated into full-length toxin. One variant achieved near-wild-type paralytic potency and a 300% reduction in antidrug antibody response *in vivo*. Thus, we have achieved a striking level of BoNT/A-LC functional deimmunization by combining computational library design and ultrahigh-throughput screening. This strategy holds promise for deimmunizing other biologics with complex superstructures and mechanisms of action.

KEYWORDS: *deimmunization, computational library, botulinum neurotoxin, FACS*

INTRODUCTION

Botulinum neurotoxin serotype A (BoNT/A) is a potent neurotoxin approved for both cosmetic and therapeutic applications, the latter including disorders of the neuromuscular system, ophthalmic system, lower urinary tract, gastrointestinal system, and others.[1−3] Despite the neurotoxin's widespread success as a drug, immunogenicity issues in therapeutic contexts have been reported, especially for medical indications involving relatively high doses of toxins.[4−7] Antidrug antibodies (ADA) directed against BoNT/A have been observed in therapeutic studies for the past several decades,[8,9] and neutralizing ADAs compromise BoNT/A's efficacy and can result in treatment failure.[10,11]

BoNT/A is composed of a 100 kDa heavy chain (BoNT/A-HC) that is linked to a 50 kDa light chain (BoNT/A-LC) via a disulfide bond (Figure S1).[12] BoNT/A-HC includes both the receptor-binding domain, which targets neuronal cell surface receptors and mediates cell entry, and the translocation domain, which facilitates toxin escape into the cytoplasm from acidified endosomal vesicles. Activated BoNT/A-LC is a zinc protease that, upon translocation to the cytoplasm, hydrolyzes soluble *N*-ethylmaleimide-sensitive factor attachment protein receptors (SNAREs), such as synaptosomal-associated protein (SNAP-25),[13] thus disrupting neurotransmitter release causing muscle paralysis.[14−16] Human subjects can develop neutralizing ADAs directed against BoNT/A-LC,[17] and previous studies suggest that helper T cell epitopes embedded in the BoNT/A-LC sequence are

Received: August 5, 2022
Published: January 9, 2023

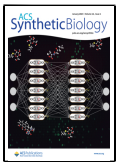

https://doi.org/10.1021/acssynbio.2c00426
ACS Synth. Biol. 2023, 12, 153−163

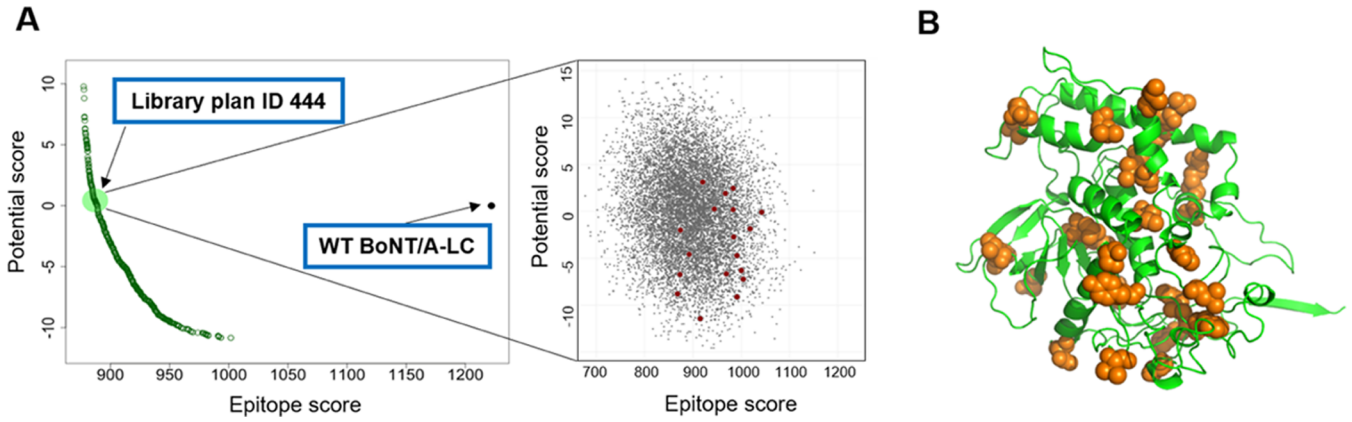

Figure 1. Generation of computationally designed, deimmunized BoNT/A-LC libraries. (A) Deimmunized libraries of BoNT/A-LC were designed using a structure-based potential score (normalized to WT) and NetMHCIIpan-based T cell epitope score. The average scores for a Pareto optimal series of libraries are plotted in green. Library plan ID 444 was chosen for high-throughput screening. The inset shows the scores for randomly sampled library variants (gray dots) as well as 18 specific variants isolated by ultrahigh-throughput FACS screening (red circles). (B) Crystal structure of the BoNT/A-LC polypeptide backbone as a green ribbon (RCSB ID: 3BTA) with mutationally targeted residues of library plan ID 444 shown as orange spheres.

partly responsible for driving the anti-BoNT/A ADA response.[18] These T cell epitopes are short peptide fragments that are proteolytically processed from foreign protein antigens, displayed on the surface of professional antigen-presenting cells in complex with class II MHC, and surveilled by cognate T cell receptors on the surface of $CD4^+$ helper T cells.[19] Formation of MHC II−peptide−T cell receptor complexes activates $CD4^+$ T cells, which go on to drive antibody affinity maturation and class-switching among antigen-specific B cells. Thus, potent ADA responses are fundamentally driven by $CD4^+$ T cell help, and while much is known about the anti-BoNT/A immune response, this knowledge has yet to be leveraged toward engineering less immunogenic BoNT/A variants.

Biotherapeutic immunogenicity can be mitigated by "deletion" of a protein drug's constituent T cell epitopes, i.e., introducing mutations in the biotherapeutic's sequence to reduce binding of its constituent peptides by class II MHC. If successful, T cell epitope deletion can silence $CD4^+$ T cell activation and, as noted above, dampen the ADA response against the offending biotherapeutic.[20] Importantly, there are increasingly accurate and facile computational tools for predicting a protein's component T cell epitopes,[21] but casual mutagenesis of predicted epitopes can undermine protein stability, activity, and overall fitness. Large and complex molecules such as BoNT/A are especially challenging,[22] as a greater mutational load is necessary to effect protein-wide T cell epitope deletion, yet their multidomain structures and multistage mechanisms of action may be acutely sensitive to mutational effects.

As a first step toward BoNT/A deimmunization, we sought to delete T cell epitopes from the BoNT/A-LC protease domain. To do so, we utilized our EpiSweep protein deimmunization algorithm, which employs structure-based design to optimally balance mutational T cell epitope deletion against retention of protein stability and activity.[23] To further improve the probability of success with this challenging target, we elected to pursue a combinatorial library-based approach, wherein an ensemble of deimmunized candidates is designed to cover a wide swath of sequence space, trading off the extent of protein deimmunization with predicted protein fitness.[24] The libraries were subjected to a single-cell, ultrahigh-throughput screen, and isolated BoNT/A-LC variants were tested for activity and immunogenicity both *in vitro* and *in vivo*. The results highlight the utility of our computationally driven, library-based approach to biotherapeutic deimmunization and demonstrate the feasibility of deimmunizing complex biotherapeutic superstructures, such as BoNT/A.

RESULTS

Generation of Computationally Designed, Deimmunized BoNT/A-LC Libraries. Both previous experimental mapping[25] and our own NetMHCIIpan[26] computational predictions revealed numerous distributed T cell epitopes throughout the BoNT/A-LC sequence, suggesting that a high mutational load might be required for effective deimmunization. However, full-length BoNT/A is a complex multidomain protein requiring precise integration of the light chain with the two heavy-chain domains,[12,27] and the biologically active ensemble manifests a sophisticated, multistage mechanism of action entailing molecular homing to nerve cell surface receptors, receptor-mediated cell uptake, endosomal activation, endosomal escape, and ultimately catalytic cleavage of SNARE substrates.[3] Thus, there is a substantial risk that high mutational loads targeting broadly distributed T cell epitopes could disrupt the toxin's native structure or biological activity.

To mitigate the risk of BoNT/A destabilization or inactivation due to aggressive re-engineering, we implemented a library-based design strategy using our previously published EpiSOCoM algorithm.[23] EpiSOCoM chooses both target positions and alternative amino acids at those positions so that a library composed of all combinations of these possibilities will be enriched in variants predicted to be functionally deimmunized (i.e., acceptable in terms of both structural integrity and immunogenicity risk). To improve overall library fitness, residues on the BoNT/A-LC that contact the BoNT/A-HC domains or the SNAP-25 substrate[28] were fixed as nonmutable (Table S1). Next, candidate mutations were derived from statistical analysis of residues in a redundancy-reduced set of BoNT/A-LC homologs. Position-specific substitutions were deemed allowable if they exceeded background frequencies in the homolog set.[29] The allowed

https://doi.org/10.1021/acssynbio.2c00426
ACS Synth. Biol. 2023, 12, 153−163

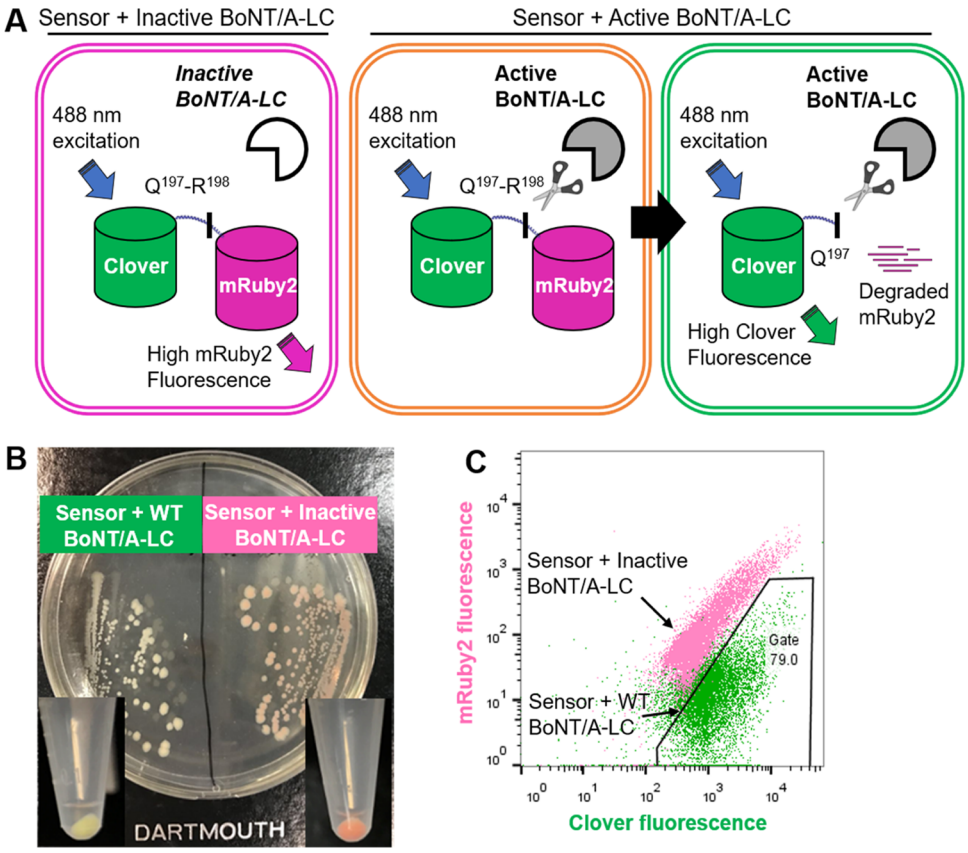

Figure 2. Development of a FRET sensor system for BoNT/A-LC activity. (A) A FRET sensor system (Clover-SNAP25-mRuby2) was utilized to efficiently measure the catalytic activity of BoNT/A-LC variants. The Clover-mRuby2 FRET pair is linked by the BoNT/A-targeted C-terminal SNARE domain of SNAP-25 (residues 141−206). When the FRET sensor is co-expressed with inactive BoNT/A-LC in *E. coli* and excited at 488 nm, a FRET signal from mRuby2 can be measured. When the FRET sensor is co-expressed with active BoNT/A-LC, the targeted SNAP-25 linker is cleaved by the protease and the FRET signal from mRuby2 is diminished. (B) Expression host phenotypic differences are observable when the sensor is co-expressed with either active WT BoNT/A-LC or inactive BoNT/A-LC. (C) Cells expressing the FRET sensor and either active WT BoNT/A-LC or inactive BoNT/A-LC exhibit clear spectral separation when measured by flow cytometry.

mutations and their combinations were scored using a structure-based sequence potential,[24] to assess structural fitness, along with the NetMHCIIpan T cell epitope predictor to assess immunogenicity risk. Finally, the pre-computed sequence potential and immunogenicity predictions were used to design a Pareto optimal series of deimmunized combinatorial libraries via our EpiSOCoM algorithm.[23] Alternative library choices along the Pareto frontier of the design space exhibited differing trade-offs between extent of T cell epitope reduction and maintenance of structural integrity (Figure 1A). For an even more in-depth description of the algorithm's workflow and implementation, the reader is directed to our published methods.[23]

Deimmunized library plan ID 444 was chosen for screening, as it maintained an average potential score (−0.05) similar to that of wild-type (WT) BoNT/A-LC but possessed substantially reduced T cell epitope content over the library ensemble (min/mean/max epitope scores = 586/892/1231, respectively; WT epitope score = 1222). This library plan specifies 28 mutable positions (Figure 1B) and associated amino acid substitutions, yielding a theoretical diversity of 268 million unique variants over all different combinations of mutational choices (Table S2).

Development of a FRET Sensor System for BoNT/A-LC Activity. To efficiently screen our deimmunized BoNT/A-LC library, a fluorescent protein-based FRET sensor for measuring BoNT/A-LC catalytic activity was adapted to enable fluorescent activated cell sorting (FACS) in bacterial expression hosts. This FRET sensor is composed of a Clover-mRuby2 FRET pair[30,31] genetically fused via a fragment of the SNAP-25 substrate.[32−35] In this FRET system, inactive BoNT/A-LC variants leave the SNAP-25 linker intact and produce high relative mRuby2 (acceptor) signal following excitation of Clover (donor). Conversely, in the presence of active BoNT/A-LC, the SNAP-25 linker is cleaved between Q197 and R198,[36] separating the donor−acceptor fluorescent proteins and eliminating FRET. Additional spectral separation of active and inactive BoNT/A-LC results from degradation of the mRuby2 acceptor due to proteolysis via the "N-end rule"[32,37] (Figure 2A).

To validate this system, the FRET sensor was tested in *E. coli* with both WT BoNT/A-LC and an inactive BoNT/A-LC control, where the latter contains two mutations that greatly reduce enzymatic activity.[28] When the sensor was co-expressed with the BoNT/A-LC controls in *E. coli*, the cells containing inactive BoNT/A-LC were visibly red, while cells with active WT BoNT/A-LC instead exhibited a characteristic GFP-green hue (Figure 2B). WT and inactive BoNT/A-LC cell populations were quantitatively analyzed via flow cytometry, where the spectral separation enabled gating that captured approximately 80% of the WT and less than 0.1% of the inactive BoNT/A-LC population (Figure 2C). These results

https://doi.org/10.1021/acssynbio.2c00426
ACS Synth. Biol. 2023, 12, 153−163

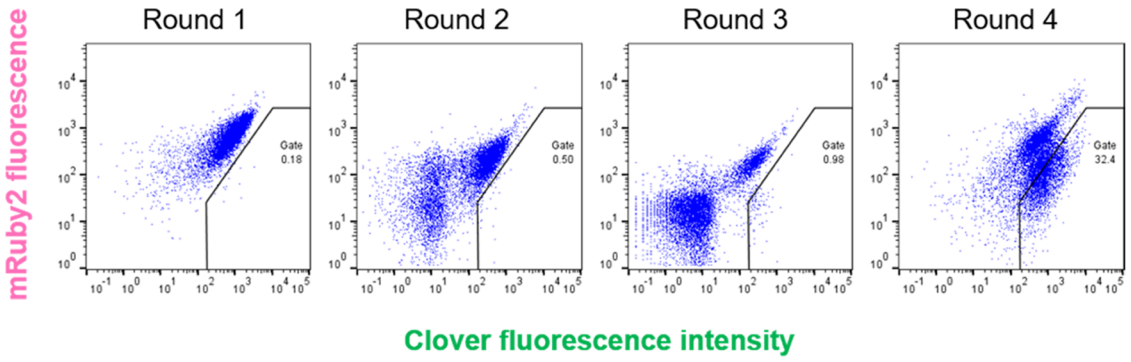

Figure 3. Ultrahigh-throughput screening of deimmunized BoNT/A-LC library. Deimmunized library plan ID 444 was co-expressed with the Clover-SNAP25-mRuby2 FRET sensor in *E. coli* BL21 (DE3) and functional variants were enriched by sorting for high clover and low mRuby2 signals during four successive rounds of FACS. Representative sort gates and the percentage of gated cells are shown (round 1 = 0.18%; round 2 = 0.50%; round 3 = 0.98%; round 4 = 32.4%).

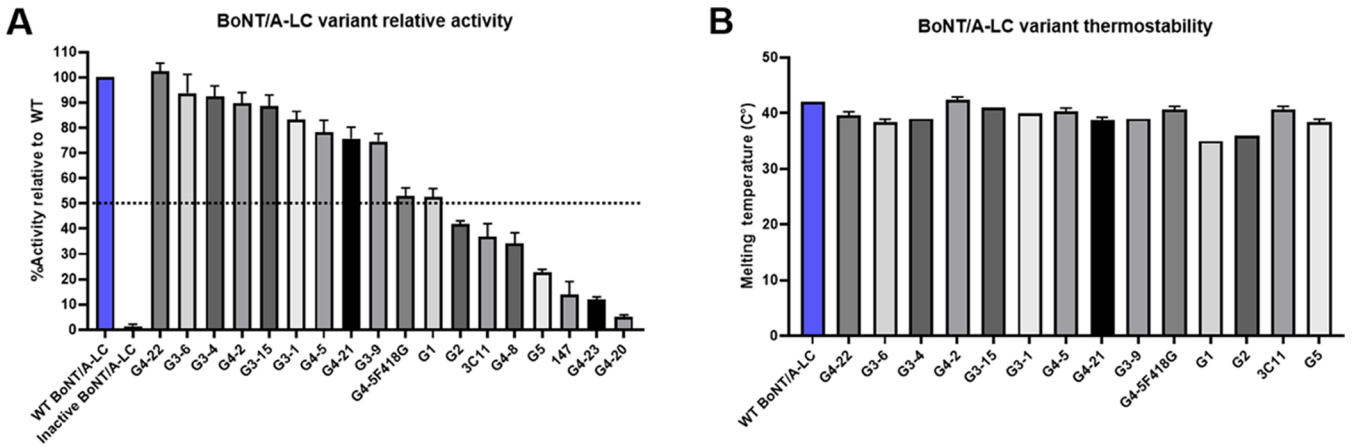

Figure 4. *In vitro* catalytic activity and thermal stability of deimmunized BoNT/A-LC variants. (A) Relative activity was analyzed by incubating purified BoNT/A-LC variants with purified Clover-SNAP25-mRuby2 FRET sensor, exciting with 488 nm light, and measuring the ratio of Clover signal (emission at 525 nm) to mRuby2 signal (emission at 600 nm) over time. Specific activity was defined as the rate of change of the Clover to mRuby2 emission ratio in the linear region of the time course. Shown are average rates normalized to WT BoNT/A-LC (n = 3−9). The hatched line indicates 50% WT BoNT/A-LC activity. (B) Thermostability of the truncated variants measured using differential scanning fluorimetry (n = 3).

indicated that the FRET sensor was suitable for ultrahigh-throughput library screening via FACS.

Importantly, the FRET sensor also enabled *in vitro* kinetic measurements of purified BoNT/A-LC enzymes. Upon excitation with 488 nm light, purified FRET sensor incubated with WT BoNT/A-LC exhibits a rapid loss of mRuby2 signal (600 nm emission, Figure S2A) and a corresponding rapid increase in Clover signal (525 emission, Figure S2B). In contrast, FRET sensor incubated with inactive BoNT/A-LC exhibits a smaller and more gradual mRuby2 signal reduction and no increase in Clover signal. To control for photobleaching effects, a ratiometric signal (Em 525/Em 600) was measured and plotted as a function of time, enabling the determination of enzyme-specific activity (Figure S2C).

Ultrahigh-Throughput Screening of Deimmunized BoNT/A-LC Library. The Clover-SNAP25-mRuby2 FRET sensor was co-expressed with the deimmunized BoNT/A-LC library and clones producing active BoNT/A-LC variants were isolated by sorting on low relative mRuby2 signal and high Clover signal (Figure 3). Round 1 sorted cells were cultured, re-induced, and rescreened with a similar gate to isolate a round 2 population, which was found to exhibit an unexpectedly high fraction of nonfluorescent cells. This nonfluorescent population was thought to be the result of cytotoxicity due to fluorescent protein overexpression.[38] To mitigate this issue, plasmid was isolated from the round 2 population and re-transformed into fresh *E. coli* prior to the round 3 sort. The round 3 sorted cells exhibited some enrichment of the target cell population; however, the nonfluorescent subpopulation persisted. Therefore, genes from the round 3 sorted cells were subcloned into fresh vector backbone and re-transformed prior to the round 4 sort. This re-cloning step eliminated the nonfluorescent subpopulation and yielded a substantial fraction of cells falling within the target sort gate. The round 4 sorted cells were plated directly onto agar induction medium, and colonies exhibiting GFP fluorescence under a blue LED light source were harvested. Notably, genes from the isolated cells collectively encoded 27 of the 28 designed mutations from library ID 444 (Table S3), highlighting the predictive power of the EpiSOCoM design algorithm.

***In Vitro* Characterization of Deimmunized BoNT/A Variants.** Eighteen of the isolated BoNT/A-LC variants were selected for additional *in vitro* characterization. To promote soluble expression of the pure variants, each construct was truncated to remove a C-terminal unpaired cysteine (C430)

https://doi.org/10.1021/acssynbio.2c00426
ACS Synth. Biol. 2023, 12, 153−163

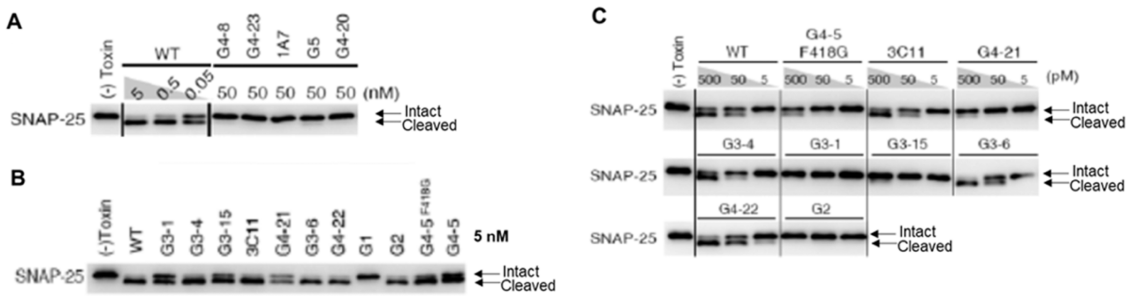

Figure 5. *In vitro* potency of full-length BoNT/A variants. Neurotoxin biological activity as measured by variant-mediated SNAP-25 cleavage in rat cortical neurons after 12 h treatment with full-length BoNT/A variants at the indicated concentrations. SNAP-25 cleavage was detected by western blot. (A) WT BoNT/A exhibited activity in a dose-dependent manner between 0.05 and 5 nM, while other variant constructs had negligible activity at a higher 50 nM concentration. (B) At 5 nM, five of the variants exhibited WT-like SNAP-25 cleavage (G3-4, 3C11, G3-6, G4-22, and G2). (C) Activity in the picomolar range was also detectable for six of the tested variants (G4-5F418G, 3C11, G4-21, G3-4, G3-6, and G4-22).

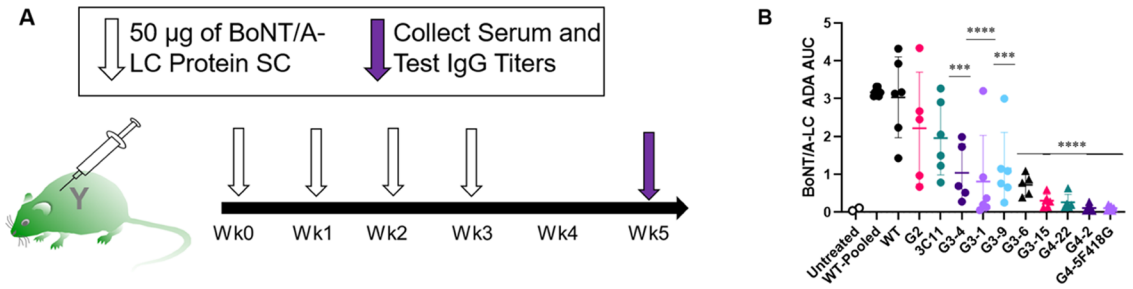

Figure 6. *In vivo* immunogenicity of BoNT/A-LC variants. (A) Transgenic DR4 mice were challenged with 4 weekly 50 μg subcutaneous doses of select BoNT/A-LC variants, and serum was collected at week 5 (n = 5−6 per group). (B) Terminal plasma was tested for antidrug antibodies by indirect ELISA against the corresponding variant antigen, and ELISA area under the curve (AUC) was calculated for each individual mouse (**** for $P \leq 0.0001$ and *** for $P \leq 0.001$, one-way ANOVA, Dunnett comparison to WT BoNT/A-LC control).

that might otherwise have resulted in unwanted disulfide-mediated dimerization. Truncated genes were cloned into a pET26b vector, expressed in *E. coli* BL21 (DE3), and purified by immobilized metal affinity chromatography (IMAC).

Specific activities of the truncated BoNT/A-LC variants were measured by incubation with a purified FRET sensor (Figure 4A). BoNT/A-LC variant G4-22 exhibited WT activity, while 10 of the other 18 variants retained greater than 50% of WT activity. Interestingly, eight well-tolerated mutations were encoded by most of these high-activity variants (Q30E, N81A, S156G, L283D, Q310D, V354S, A371G, and T413D, Table S3). Melting temperatures (T_m) for the 15 most active variants were subsequently measured by differential scanning fluorimetry (DSF), and all were found to be within approximately 3 °C of WT (Figure 4B).

To assess activity in a more biologically relevant manner, full-length toxins were assembled *in vitro* using a previously established sortase-mediated ligation strategy.[39−41] Briefly, two nontoxic fragments of BoNT/A are recombinantly produced in *E. coli*. One fragment contains the BoNT/A-LC, the translocation domain, and a C-terminal short peptide sequence that can be recognized by sortase. The second fragment contains the receptor-binding domain with an N-terminal thrombin cleavage site. These two fragments can be produced separately and ligated together using sortase to form a full-length, functional toxin (Figure S3). The biological activities of the full-length toxins were evaluated by measuring toxin-mediated SNAP-25 cleavage in cultured rat cortical neurons. A qualitative assessment of BoNT/A variant activity was performed by immunoblot assay. Five of the variants exhibited little to no detectable activity even at a high concentration of 50 nM (Figure 5A). At 5 nM, five of the deimmunized variants manifested activity similar to WT BoNT/A (Figure 5B). Variant toxins 3C11, G3-6, and G4-22 were further found to retain WT-like activity at low picomolar concentrations, while variants G4-5F418G, G4-21, and G3-4 exhibited weaker but detectable activity at higher picomolar concentrations (Figure 5C). In summary, the high-throughput library screen yielded numerous variants that exhibited a range of biological activities, which in some cases were similar to WT BoNT/A. Select variants exhibiting cell-based *in vitro* activity were further characterized in murine models of immunogenicity and potency.

***In Vivo* Immunogenicity of BoNT/A-LC Variants.** The BoNT/A-LC library was optimized to delete $CD4^+$ helper T cell epitopes with the goal of reducing ADA responses in human subjects. Because the design process specifically targeted T cell epitopes restricted by human class II MHC, preclinical assessment of the variants' reduced immunogenicity necessitated testing in humanized HLA transgenic mice. Specifically, we employed DR4 transgenic mice expressing a chimeric MHC II protein in which the peptide binding domains are derived from human MHC II allele DRB1*0401,[42] a representative human MHC-II supertype.[43]

To assess *in vivo* immunogenicity, DR4 mice were immunized once weekly for 4 weeks with select BoNT/A-LC proteins (Figure 6A). Plasma was collected 2 weeks after the final immunization, and anti-BoNT/A-LC IgG antibody titers were determined by indirect ELISA. WT BoNT/A-LC was found to be strongly immunogenic, with an average ADA area under the curve (AUC) of 3.04. All 10 tested variants elicited lower average ADA titers relative to WT, falling broadly into one of three categories (Figure 6B, Table S3, Figure S4). Variants G-2 and 3C11 exhibited strong residual immunoge-

https://doi.org/10.1021/acssynbio.2c00426
ACS Synth. Biol. 2023, 12, 153−163

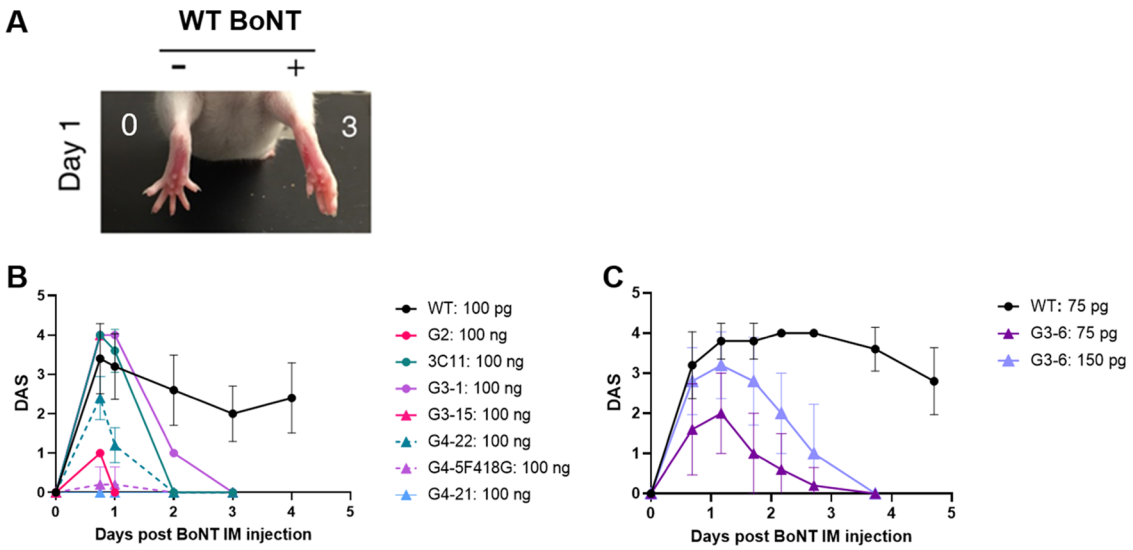

Figure 7. *In vivo* activity of reconstituted full-length BoNT/A variants. (A) Paralytic activity of BoNT/A-LC variants incorporated into full-length toxins was quantified as a Digit Abduction Score (DAS) in a murine flaccid paralysis model. No activity corresponds to zero abducted digits (left limb) and max activity corresponds to four abducted digits; see right limb for DAS = 3. (B) CD-1 mice were challenged locally by intramuscular (IM) injection of BoNT/A-LC variant-containing toxins, and DAS response was measured for up to 4 days (n = 5 per group). For the majority of tested variants, muscle weakening was observed; however, potency was found to be at least 1000-fold lower than WT BoNT/A. (C) For deimmunized variant G3-6, potency was more comparable to WT; however, the variant's duration of action was shorter (n = 5 per group).

nicity, with only a trend toward lower ADA than WT. Variants G3-4, G3-1, G3-9, and G3-6 demonstrated weak residual immunogenicity that was significantly lower than WT (one-way ANOVA, Dunnett comparison to WT BoNT/A-LC control). Variants G3-15, G4-22, G4-2, and G4-5F418G were even more deimmunized, eliciting little to no ADA response. Notably, the correlation coefficient between the variants' DRB1*0401-specific epitope score and their ADA response in DR4 mice was significantly nonzero (Figure S5), highlighting the general utility of designed-based T cell epitope deletion.

***In Vivo* Activity of Full-Length BoNT/A Variants.** To assess the deimmunized variants' capacity to manifest paralytic activity, reconstituted full-length toxins containing either the WT or deimmunized BoNT/A-LCs were tested in a murine model of flaccid paralysis. Specifically, variant-containing toxins were injected into the right hind limbs of mice, and muscle weakening was quantified as a digit abduction score (DAS), or the number of rear digits that mice failed to reflexively spread on the associated hind limb (Figure 7A).[44]

WT BoNT/A dosed at 100 pg manifests strong paralytic activity for more than 4 days (Figure 7B). Of the eight variant-containing toxins tested, G4-5F418G and G4-21 exhibited low to negligible activity at a dose of 100 ng, or 1000-fold higher dosing than WT. Variants G2 and G4-22 exhibited marginal activity at 100 ng. Variants 3C11, G3-1, and G3-15 manifested stronger *in vivo* activity at 100 ng, achieving a maximum paralytic effect similar to that of WT BoNT/A dosed at 100 pg. However, their duration of action remained less than that of wild-type BoNT/A, despite their 1000-fold higher dosing. In contrast to other deimmunized candidates, variant G3-6 exhibited far greater paralytic activity, effecting notable paralysis for more than 2 days at a dose of only 75 pg (Figure 7C). At 150 pg, G3-6 demonstrated peak paralytic activity close to that of WT BoNT/A dosed at 75 pg, though as with other variants, G3-6 also exhibited an abbreviated duration of action.

DISCUSSION

Immunogenicity risk is an important consideration in the development of biotherapeutics, as ADAs can impact both drug safety and efficacy.[45,46] A therapeutic protein's origin is one risk factor for immunogenicity, where nonhuman proteins may be predisposed toward greater immunogenicity, especially when dosed repeatedly.[47] BoNT/A is one such biotherapeutic of microbial origin that is known to elicit neutralizing ADAs in human patients.[4,48] Thus, development of BoNT/As with reduced immunogenicity is of particular interest.

Mutagenic deletion of $CD4^+$ helper T cell epitopes is one strategy for mitigating biotherapeutic immunogenicity and suppressing ADA responses during repeated drug dosing. Importantly, T cell epitope-deleting mutations must be compatible with the protein's native fold and therapeutic function.[20,49] Addressing the immunogenicity of multidomain biotherapeutics poses a particular challenge, due to the interconnected contributions of each domain to protein structure, function, and immunogenicity risk.[22] We have previously shown that computationally driven design of deimmunized libraries coupled with high-throughput functional screening can generate T cell epitope depleted candidates that evade human T cell surveillance,[50] suppress antidrug antibody responses,[51,52] yet retain high-level efficacy. Here, we explored the potential for our structure-based library design strategies[23,24] to yield deimmunized BoNT/A-LC variants that remained competent to assemble full-length and biologically active neurotoxins.

The complexity of BoNT/A's structure−function−immunogenicity relationships has to date precluded any significant progress in deimmunizing this powerful biotherapeutic. By leveraging Pareto optimal protein design algorithms, we created a series of deimmunized library options that differentially balanced the predicted trade-offs between immunogenicity vs stability and activity (Figure 1A). Importantly, when pursuing a library-based approach, a single design yields a combinatorial ensemble of variants that efficiently explores

https://doi.org/10.1021/acssynbio.2c00426
ACS Synth. Biol. 2023, 12, 153−163

trade-offs in immunogenicity vs protein fitness. We speculated that by sampling a diverse sequence space containing variants from low to high mutational loads, we would find BoNT/A-LC variants with a desirable combination of performance and immunological characteristics.

The designed library comprised approximately 270 million distinct deimmunized BoNT/A-LC variants, and we leveraged an ultrahigh-throughput FACS screening strategy to isolate rare functional clones from this large population. While low-mutation variants are inherently more likely to retain WT stability and activity, our 18 isolated candidates exhibited high average mutational loads (11.6 residues per protein), demonstrating that the design algorithm effectively identified multimutation sets that were biased toward retention of BoNT/A-LC activity.

Among the isolated library members characterized in more detail, we observed a range of catalytic rates for truncated BoNT/A-LC, *in vitro* full-length toxin activity, *in vivo* full-length toxin paralytic efficacy, and *in vivo* BoNT/A-LC immunogenicity in human HLA transgenic mice. For example, variant G4-5F418G was essentially nonimmunogenic in DR4 mice (Figures 6B and S4), but compared to WT BoNT/A it was more than 1000-fold less potent as a full-length toxin (Figure 7B). Alternatively, variant 3C11 exhibited *in vivo* activity at 100 ng (Figure 7B) but achieved only a 50% reduction in ADA response in DR4 mice (Figures 6B and S4). Variant G3-6 on the other hand struck a more favorable balance between measured efficacy and immunogenicity, exhibiting near WT activity both *in vitro* and *in vivo* while achieving a >300% reduction in ADA response. The trade-offs observed in our isolated variants underscore the utility of our ensemble approach to biotherapeutic deimmunization. Specifically, computational design of a deimmunized library followed by high-throughput functional screening can produce a panel of active candidates, and variants that optimally balance various performance metrics may be chosen from such a functionally enriched panel.

Although this study represents an important step toward development of a low immunogenicity BoNT/A therapy, there are several limitations to acknowledge. First, this study sought to engineer only the BoNT/A-LC, while it is known that the BoNT/A-HC, comprising the receptor-binding and translocation domains, also contains immunogenic T cell epitopes and is the antigenic target of some antibodies.[53−55] Thus, a fully deimmunized BoNT/A will require analogous engineering of the heavy chain. Additionally, while we optimized the BoNT/A-LC for reduced T cell epitope content restricted by diverse human HLA alleles, the immunogenicity of our candidates was tested only in DR4 mice, which encode the single DRB1*0401 HLA supertype, and only under a single immunization schedule. Therefore, additional studies will be required to assess the extent to which our variants dampen ADA responses driven by other HLA alleles and under other dosing regimens. Importantly, however, we have shown in prior studies that optimization against a representative set of human HLA supertypes, as executed here, results in deimmunized proteins that are broadly evasive of diverse human HLA.[50,52]

Second, BoNT/A toxins produced via sortase-mediated ligation have been observed to have reduced potency compared to natively generated toxin,[41] and thus the cell-based and *in vivo* activities reported here for full-length toxins do not represent their inherent potency. Instead, the sortase-ligated toxins described here served as surrogates by which to validate the variant light chains' capacity to act upon neurons following targeting and delivery via the wild-type BoNT/A receptor-binding and translocation domains. All comparisons among variant light chains were done within the same context (all were sortase-ligated), with the only difference being the sequences of the light chains themselves. As part of any future drug development effort, the potency, pharmacokinetics, and pharmacodynamics of our mutated toxins would have to be tested with material produced directly as full-length proteins.

Finally, we note that even our top-performing variant G3-6 suffered from reduced duration of action compared to WT BoNT/A. This suggests that the variant would require more frequent dosing than the WT toxin, which can retain paralytic activity for ≥3 months in humans.[56] On the other hand, a reduced duration of action might be favorable in certain applications. For example, BoNT/A treatment of pain associated with short-term injury would benefit from limited duration of action, permitting redosing on an as-needed basis.

In conclusion, we have employed computational optimization to design large deimmunized libraries of BoNT/A-LC, and we have leveraged an ultrahigh-throughput FACS screen to isolate highly active, highly mutated, and strongly immunoevasive BoNT/A-LC variants. This achievement highlights the power of our computationally driven, library-based approach to biotherapeutic deimmunization, and it points the way toward achieving functional deimmunization of other biotherapeutics having large and complex superstructures that function via multistage mechanisms of action.

METHODS

Generation of Computationally Designed Deimmunized BoNT/A-LC Libraries. Deimmunized libraries of the BoNT/A-LC (residues 1−448) were generated by first identifying nonmutable residues known or expected to be functionally or structurally important. These nonmutable sites include interface residues between the BoNT/A heavy and light chains as well as enzymatic active site residues. Potential mutations (excluding cysteines and prolines) for the remaining mutable sites were generated from homolog sequences pulled from a BLAST sequence alignment and pre-processed for structural stability as well as peptide immunogenicity. Structural stability is represented by a potential score based on a cluster expansion (CE) technique that predicts structural energies of sequence variants.[24] Peptide immunogenicity is represented by an epitope score based on predicted MHC-II peptide binding affinity covering 27 MHC-II HLA alleles.[26] Finally, the structural potential and immunogenicity scores are used to generate deimmunized combinatorial libraries along a Pareto optimal curve.[57] A total of 508 deimmunized ALC libraries were computationally designed along the Pareto optimal curve, of which Library ID 444 was selected for screening and synthesized by Synbio Technologies.

Development of a FRET Sensor System for BoNT/A-LC Libraries. The Clover-SNAP25-mRuby2 FRET sensor system was generated from an initial Clover-mRuby2 construct provided by the Dong Lab at Boston Children's Hospital. SNAP-25 residues 141−206 were inserted between the Clover-mRuby2 FRET pair to complete the sensor system and cloned into pRSF-Duet and pET26b vector systems by Gibson Assembly. WT BoNT/A-LC and inactive BoNT/A-LC (double-mutant E244Q, T366F) were also cloned into pRSF-Duet and pET26b vector systems by Gibson Assembly.

https://doi.org/10.1021/acssynbio.2c00426
ACS Synth. Biol. 2023, 12, 153−163

Cell-based FRET sensor characterization was performed by transforming *E. coli* BL21 (DE3) with the co-expressed FRET sensor and either active or inactive BoNT/A-LC in the pRSF-Duet vector. These co-expressed cells were then grown on selective agar plates with 0.1 mM isopropyl-β-D-thiogalactopyranoside (IPTG, Research Products International) or in Luria Broth (LB, Research Products International) media followed by 0.1 mM IPTG induction. Clover fluorescence was measured at 488 nm excitation and 525 nm emission while mRuby2 FRET fluorescence was measured at 585 nm emission.

Ultrahigh-Throughput Screening of Deimmunized BoNT/A-LC Library. The deimmunized library ID 444 was cloned into the pRSF-Duet vector along with the FRET sensor and transformed into *E. coli* BL21 (DE3). Cells were grown in selective LB media and induced with 0.1 mM IPTG before fluorescence-activated cell sorting (488 nm excitation, 525/50 nm emission, 585/40 nm emission). Sorted cells falling in the low mRuby2 sort gate were grown overnight, subcultured, and induced with 0.1 mM IPTG before the next round of sorting. After the second round of sorting, plasmid was isolated and re-transformed into fresh *E. coli* BL21 (DE3). After the third round of sorting, subcloning was employed by PCR amplifying the enriched library followed by cloning into fresh pRSF-Duet vector with the FRET sensor, and subsequent re-transformation into fresh *E. coli* BL21 (DE3). After the fourth round of sorting, cells enriched for low mRuby2 signal and positive Clover signal were plated on selective LB agar with 0.1 mM IPTG. Select colonies exhibiting high Clover and low mRuby2 signal under a blue LED light were chosen for additional characterization.

***In Vitro* Catalytic Activity and Thermostability of Deimmunized BoNT/A-LC Variants.** *In vitro* characterization of the enriched deimmunized BoNT/A-LC variants was performed using truncated (residues 1−424) versions and FRET sensor cloned into pET26b vector. Truncated BoNT/A-LC variants (with C-terminal His-tags) were amplified using a forward primer 5′- TTTAACTTTAAGAAGGAGATATACATATGGCATTCGTCAACAAACAGTTCAA-3′ and reverse primer 5′-CAGTGGTGGTGGTGGTGGTGCTCGAGGAACTCGAACAGGCCGGTGAAGT-3′. The FRET sensor (with C-terminal His-tag) was amplified using a forward primer 5′-TTTAACTTTAAGAAGGAGATATACATATGATCAAGGAAAATATGCGTATGAAG-3′ and reverse primer 5′-CAGTGGTGGTGGTGGTGGTGCTCGAGGGCGGCGGTCACGAACTCCAGCA-3′. In addition to the variants produced from the deimmunized library screen, G4-5F418G was constructed by inserting an F418G mutation into variant G4-5 to further reduce the potential immunogenicity based on computational analysis. These truncated variants as well as the FRET sensor were transformed into *E. coli* BL21 (DE3), grown in selective LB media, and induced with 0.1 mM IPTG. Cells were then pelleted and resuspended in phosphate-buffered saline (PBS) before physical cell lysis using a cell sonicator (Fisher Sonic Dismembrator). The soluble cell lysate was filtered through a 0.22 μm filter unit, and the 6× histidine-tagged variants were purified by immobilized metal ion affinity chromatography (IMAC).

To measure relative catalytic activity, 8 nM of purified WT BoNT/A-LC, inactive BoNT/A-LC, or deimmunized BoNT/A-LC variants were incubated with 67 nM of purified Clover-SNAP25-mRuby2 FRET sensor in reaction buffer (50 mM Trish-HCl, 10 μM $ZnCl_2$, pH 7.2) on a 96-well plate (n = 3−9 distinct samples). The ratio of Clover fluorescence (488 nm excitation, 525 nm emission) to mRuby2 FRET fluorescence (600 nm emission) was measured for 60 min and the slope was calculated over the linear portion of the time course. The slope representing the catalytic activity of each BoNT/A-LC variant was normalized to the WT measurement to calculate a relative catalytic activity. Fluorescence measurements were performed in a Corning 96-well black-sided polystyrene microplate using a SpectraMax Paradigm multimode microplate detection plate reader.

Thermostability of each BoNT/A-LC variant was determined by differential scanning fluorimetry (DSF).[58] For each purified BoNT/A-LC variant (n = 3 distinct samples), 5 μM was incubated with 5× SYPRO Orange dye (Invitrogen) and subjected to a temperature gradient from 25 to 99 °C at 1 °C per minute steps using a real-time PCR detection system. Melting temperatures were calculated using the Bio-Rad CFX Manager 3.0 software. Here, the rate of change in fluorescence as a function of temperature is assessed, with the protein unfolding transition (T_m) being represented by the highest rate of change observed.

Full-Length BoNT/A Production and *In Vitro* Activity. Full-length BoNT/A was produced by first creating a fusion construct of the WT or deimmunized BoNT/A-LC variants with the WT heavy-chain translocation domain via a thrombin cleavage site (LVPR/GS), and appended with a C-terminal sortase cleavage motif (LPETGG). Separately, the WT heavy-chain receptor-binding domain is constructed with an N-terminal thrombin cleavage motif. These constructs are expressed in *E. coli* and purified via IMAC. The purified WT heavy-chain receptor-binding domain was thrombin treated (to expose an N-terminal glycine) and then incubated with the purified WT or deimmunized BoNT/A-LC and WT heavy-chain translocation domain fusion constructs (LCH_N, containing a C-terminal sortase motif) in the presence of sortase. The sortase transpeptidase cleaves the sortase motif and allows peptide bond formation via the exposed N-terminal glycine on the WT heavy-chain receptor-binding domain. This produces full-length BoNT/A variants via sortase ligation that can then be activated by an additional thrombin incubation (0.4 units of thrombin for 30 min at room temperature) to allow complete toxin assembly (Figure S3).[59,60]

The biological activity of full-length BoNT/A constructs was conducted by exposing cultured rat cortical neurons to the active full-length BoNT/A variants. Prenatal stage cortical tissue was isolated from rat embryos (embryonic day 18 or 19) using a papain dissociation kit (Worthington Biochemical); 1 mL of 0.25 million viable cells was seeded on each well of poly-D-lysine-coated 24-well plates, followed by 14 days culture before use. WT or deimmunized full-length BoNT/A variants were incubated with the neurons for 12 h at concentrations between 5 pM and 50 nM. To harvest lysates, the neuron cells were washed twice with PBS and lysed by adding 200 μL of lysis buffer (PBS containing 1% Triton X-100, 0.05% SDS, and protease inhibitor cocktail). SNAP-25 cleavage was analyzed via immunoblotting.

***In Vivo* Immunogenicity of BoNT/A-LC Variants.** BoNT/A-LC variant immunogenicity was tested in transgenic HLA DR4 mice. For each variant, mice (n = 5−6 per group) were challenged with 4 weekly subcutaneous doses of 50 μg of purified protein in 100 μL of sterile PBS. Control mice were treated with PBS only (n = 2). Blood was collected at week 5 via terminal, retro-orbital bleeds into heparinized capillary

https://doi.org/10.1021/acssynbio.2c00426
ACS Synth. Biol. 2023, 12, 153−163

tubes. Samples were centrifuged at 2000*g* for 10 min and the plasma was isolated. Antidrug IgG antibody titers specific to each individual variant were measured by indirect enzyme-linked immunosorbent assay (ELISA) using a standard protocol. This protocol was conducted in accordance with guidelines approved by the Institutional Animal Care and Use Committee of Dartmouth College (Hanover, NH).

***In Vivo* Activity of Full-Length BoNT/A Variants.** *In vivo* potency of full-length BoNT/A variants was tested in a murine muscle paralysis model[44] using CD-1 mice (Envigo, 5–6 weeks old, $n = 5$ per study arm). The sortase-ligated toxins were diluted into 0.2% gelatin-phosphate buffer (100 mM, pH 6.3). Diluted toxins (5 μL) containing between 75 pg and 100 ng of toxin were administered via intramuscular injection into the gastrocnemius muscle of the right hind limb using a Hamilton syringe equipped with a 30-gauge needle. The mice ($n = 5$) were randomly re-grouped to each cage before injection. Potency and toxin duration of action was measured using a Digit Abduction Score (DAS) for up to 5 days after toxin administration. The DAS observer was not blinded to treatments. This protocol was conducted in accordance with the guidelines approved by the Institute Animal Care and Use Committee (IACUC) at Boston Children's Hospital (#18-10-3794R).

Statistical Analysis. Data are given as mean ± standard deviation (SD) unless otherwise stated and analyzed using GraphPad Prism 9 for statistical analysis. Dunnett's multiple comparisons test was used for statistical group comparisons.

■ ASSOCIATED CONTENT

Supporting Information

The Supporting Information is available free of charge at https://pubs.acs.org/doi/10.1021/acssynbio.2c00426.

Nonmutable WT BoNT/A-LC residues (XLSX)

Deimmunized library ID 144 design summary; BoNT/A-LC variants enriched from the deimmunized library screen; BoNT/A complex; FRET sensor *in vitro* kinetic measurements; full-length BoNT/A generation; indirect ELISA for BoNT/A-LC variant ADA response in humanized DR4 HLA transgenic mice; and BoNT/A-LC ADA response correlation to predicted epitope score (PDF)

■ AUTHOR INFORMATION

Corresponding Author

Karl E. Griswold − *Thayer School of Engineering, Dartmouth, Hanover, New Hampshire 03755, United States;* orcid.org/0000-0002-9835-3394; Email: karl.e.griswold@dartmouth.edu

Authors

Yongliang Fang − *Thayer School of Engineering, Dartmouth, Hanover, New Hampshire 03755, United States; Department of Urology, Boston Children's Hospital, Boston, Massachusetts 02115, United States; Department of Microbiology and Department of Surgery, Harvard Medical School, Boston, Massachusetts 02115, United States*

Andrew Y. Chang − *Thayer School of Engineering, Dartmouth, Hanover, New Hampshire 03755, United States*

Deeptak Verma − *Department of Computer Science, Dartmouth, Hanover, New Hampshire 03755, United States*

Shin-Ichiro Miyashita − *Department of Urology, Boston Children's Hospital, Boston, Massachusetts 02115, United States; Department of Microbiology and Department of Surgery, Harvard Medical School, Boston, Massachusetts 02115, United States; Department of Food, Aroma and Cosmetic Chemistry, Tokyo University of Agriculture, Abashiri 099-2493, Japan*

Susan Eszterhas − *Thayer School of Engineering, Dartmouth, Hanover, New Hampshire 03755, United States*

Pyung-Gang Lee − *Department of Urology, Boston Children's Hospital, Boston, Massachusetts 02115, United States; Department of Microbiology and Department of Surgery, Harvard Medical School, Boston, Massachusetts 02115, United States*

Yi Shen − *Department of Urology, Boston Children's Hospital, Boston, Massachusetts 02115, United States; Department of Microbiology and Department of Surgery, Harvard Medical School, Boston, Massachusetts 02115, United States*

Lydia R. Davis − *Thayer School of Engineering, Dartmouth, Hanover, New Hampshire 03755, United States*

Min Dong − *Department of Urology, Boston Children's Hospital, Boston, Massachusetts 02115, United States; Department of Microbiology and Department of Surgery, Harvard Medical School, Boston, Massachusetts 02115, United States*

Chris Bailey-Kellogg − *Department of Computer Science, Dartmouth, Hanover, New Hampshire 03755, United States*

Complete contact information is available at: https://pubs.acs.org/10.1021/acssynbio.2c00426

Author Contributions

#Y.F. and A.Y.C. are co-first authors. C.B.-K. and D.V. designed the combinatorial libraries. Y.F. executed the FACS screen and completed *in vitro* characterization of isolated BoNT/A-LC variants. S.-I.M., P.-G.L., and M.D. produced the full-length toxins and conducted flaccid paralysis studies. Y.S. and M.D. designed the FRET sensor. S.E. executed ADA studies in DR4 mice. A.Y.C., Y.F., and L.R.D. analyzed the data. A.Y.C., C.B.-K., and K.E.G. wrote the manuscript, and all authors reviewed the manuscript and offered comments. K.E.G. and C.B.-K. provided funding.

Notes

The authors declare the following competing financial interest(s): KEG and CB-K are managers of Stealth Biologics, LLC, managers of Occulo Holdings LLC, and employees of Insmed Inc. YF has an equity interest in Occulo Holdings LLC. All other authors declare that they have no competing interests. Potential conflicts of interest for KEG and CB-K are under management at Dartmouth. The authors declare that the work presented here is free of any bias.

K.E.G. and C.B.-K. are managers of Stealth Biologics, LLC and Occulo Holdings LLC, and Y.F. has an equity interest in Occulo Holdings. All other authors declare that they have no competing interests. Potential conflicts of interest for K.E.G. and C.B.-K. are under management at Dartmouth. The authors declare that the work presented here is free of any bias.

■ ACKNOWLEDGMENTS

This work was supported by NIH grants (2R01GM098977 and P20-GM113132), and in part by the Defense Threat Reduction Agency (HDTRA1-20-10004 to K.E.G. and M.P.D.). *In vivo* immunogenicity studies were supported in

part by Dartmouth mouse modeling CA023108. Additional support was provided by the Dartmouth Graduate Alumni Research Award.

REFERENCES

(1) Chen, S. Clinical uses of botulinum neurotoxins: current indications, limitations and future developments. *Toxins* **2012**, *4*, 913−939.
(2) Dong, M.; Masuyer, G.; Stenmark, P. Botulinum and Tetanus Neurotoxins. *Annu. Rev. Biochem.* **2019**, *88*, 811−837.
(3) Pirazzini, M.; Rossetto, O.; Eleopra, R.; Montecucco, C. Botulinum Neurotoxins: Biology, Pharmacology, and Toxicology. *Pharmacol. Rev.* **2017**, *69*, 200−235.
(4) Bellows, S.; Jankovic, J. Immunogenicity Associated with Botulinum Toxin Treatment. *Toxins* **2019**, *11*, 491.
(5) Kumar, R.; Dhaliwal, H. P.; Kukreja, R. V.; Singh, B. R. The Botulinum Toxin as a Therapeutic Agent: Molecular Structure and Mechanism of Action in Motor and Sensory Systems. *Semin. Neurol.* **2016**, *36*, 10−19.
(6) Benecke, R. Clinical relevance of botulinum toxin immunogenicity. *BioDrugs* **2012**, *26*, e1−e9.
(7) Naumann, M.; Boo, L. M.; Ackerman, A. H.; Gallagher, C. J. Immunogenicity of botulinum toxins. *J. Neural Transm.* **2013**, *120*, 275−290.
(8) Müller, K.; Mix, E.; Adib Saberi, F.; Dressler, D.; Benecke, R. Prevalence of neutralising antibodies in patients treated with botulinum toxin type A for spasticity. *J. Neural Transm.* **2009**, *116*, 579−585.
(9) Zuber, M.; Sebald, M.; Bathien, N.; de Recondo, J.; Rondot, P. Botulinum antibodies in dystonic patients treated with type A botulinum toxin: frequency and significance. *Neurology* **1993**, *43*, 1715−1718.
(10) Dressler, D. Clinical features of antibody-induced complete secondary failure of botulinum toxin therapy. *Eur. Neurol.* **2002**, *48*, 26−29.
(11) Dressler, D. Clinical presentation and management of antibody-induced failure of botulinum toxin therapy. *Mov. Disord.* **2004**, *19*, S92−S100.
(12) Dong, M.; Stenmark, P. The Structure and Classification of Botulinum Toxins. In *Botulinum Toxin Therapy*; Handbook of Experimental Pharmacology; Springer, 2019; Vol. *263*, pp 11−33.
(13) Adler, M.; Keller, J. E.; Sheridan, R. E.; Deshpande, S. S. Persistence of botulinum neurotoxin A demonstrated by sequential administration of serotypes A and E in rat EDL muscle. *Toxicon* **2001**, *39*, 233−243.
(14) Khounlo, R.; Kim, J.; Yin, L.; Shin, Y. K. Botulinum Toxins A and E Inflict Dynamic Destabilization on t-SNARE to Impair SNARE Assembly and Membrane Fusion. *Structure* **2017**, *25*, 1679−1686.
(15) Singh, B. R. Botulinum neurotoxin structure, engineering, and novel cellular trafficking and targeting. *Neurotoxic. Res.* **2006**, *9*, 73−92.
(16) Poulain, B.; Lemichez, E.; Popoff, M. R. Neuronal selectivity of botulinum neurotoxins. *Toxicon* **2020**, *178*, 20−32.
(17) Atassi, M. Z.; Dolimbek, B. Z.; Jankovic, J.; Steward, L. E.; Aoki, K. R. Regions of botulinum neurotoxin A light chain recognized by human anti-toxin antibodies from cervical dystonia patients immunoresistant to toxin treatment. The antigenic structure of the active toxin recognized by human antibodies. *Immunobiology* **2011**, *216*, 782−792.
(18) Oshima, M.; Aoki, K. R.; Atassi, M. Z. Regions recognized on the light chain of botulinum neurotoxin type A by T lymphocytes of SJL and BALB/c mice primed with inactivated toxin. *Immunobiology* **2014**, *219*, 950−957.
(19) Roche, P. A.; Furuta, K. The ins and outs of MHC class II-mediated antigen processing and presentation. *Nat. Rev. Immunol.* **2015**, *15*, 203−216.
(20) Griswold, K. E.; Bailey-Kellogg, C. Design and engineering of deimmunized biotherapeutics. *Curr. Opin. Struct. Biol.* **2016**, *39*, 79−88.
(21) Reynisson, B.; Alvarez, B.; Paul, S.; Peters, B.; Nielsen, M. NetMHCpan-4.1 and NetMHCIIpan-4.0: improved predictions of MHC antigen presentation by concurrent motif deconvolution and integration of MS MHC eluted ligand data. *Nucleic Acids Res.* **2020**, *48*, W449−W454.
(22) Gorovits, B.; Peng, K.; Krominga, A. Current Considerations on Characterization of Immune Response to Multi-Domain Biotherapeutics. *BioDrugs* **2020**, *34*, 39−54.
(23) Choi, Y.; Verma, D.; Griswold, K. E.; Bailey-Kellogg, C.EpiSweep: Computationally Driven Reengineering of Therapeutic Proteins to Reduce Immunogenicity While Maintaining Function. In *Computational Protein Design*; Methods in Molecular Biology; Humana Press, 2017; Vol. *1529*, pp 375−398.
(24) Verma, D.; Grigoryan, G.; Bailey-Kellogg, C. Structure-based design of combinatorial mutagenesis libraries. *Protein Sci.* **2015**, *24*, 895−908.
(25) Oshima, M.; Deitiker, P.; Jankovic, J.; Atassi, M. Z. The Regions on the Light Chain of Botulinum Neurotoxin Type A Recognized by T Cells from Toxin-Treated Cervical Dystonia Patients. The Complete Human T-Cell Recognition Map of the Toxin Molecule. *Immunol. Invest.* **2018**, *47*, 18−39.
(26) Karosiene, E.; Rasmussen, M.; Blicher, T.; Lund, O.; Buus, S.; Nielsen, M. NetMHCIIpan-3.0, a common pan-specific MHC class II prediction method including all three human MHC class II isotypes, HLA-DR, HLA-DP and HLA-DQ. *Immunogenetics* **2013**, *65*, 711−724.
(27) Lacy, D. B.; Tepp, W.; Cohen, A. C.; DasGupta, B. R.; Stevens, R. C. Crystal structure of botulinum neurotoxin type A and implications for toxicity. *Nat. Struct. Biol.* **1998**, *5*, 898−902.
(28) Breidenbach, M. A.; Brunger, A. T. Substrate recognition strategy for botulinum neurotoxin serotype A. *Nature* **2004**, *432*, 925−929.
(29) McCaldon, P.; Argos, P. Oligopeptide biases in protein sequences and their use in predicting protein coding regions in nucleotide sequences. *Proteins* **1988**, *4*, 99−122.
(30) Lam, A. J.; St-Pierre, F.; Gong, Y.; Marshall, J. D.; Cranfill, P. J.; Baird, M. A.; McKeown, M. R.; Wiedenmann, J.; Davidson, M. W.; Schnitzer, M. J.; Tsien, R. Y.; Lin, M. Z. Improving FRET dynamic range with bright green and red fluorescent proteins. *Nat. Methods* **2012**, *9*, 1005−1012.
(31) Masuyer, G.; Zhang, S.; Barkho, S.; Shen, Y.; Henriksson, L.; Kosenina, S.; Dong, M.; Stenmark, P. Structural characterisation of the catalytic domain of botulinum neurotoxin X - high activity and unique substrate specificity. *Sci. Rep.* **2018**, *8*, No. 4518.
(32) Dong, M.; Tepp, W. H.; Johnson, E. A.; Chapman, E. R. Using fluorescent sensors to detect botulinum neurotoxin activity in vitro and in living cells. *Proc. Natl. Acad. Sci. U.S.A.* **2004**, *101*, 14701−14706.
(33) Garland, M.; Babin, B. M.; Miyashita, S. I.; Loscher, S.; Shen, Y.; Dong, M.; Bogyo, M. Covalent Modifiers of Botulinum Neurotoxin Counteract Toxin Persistence. *ACS Chem. Biol.* **2019**, *14*, 76−87.
(34) Binz, T.; Blasi, J.; Yamasaki, S.; Baumeister, A.; Link, E.; Sudhof, T. C.; Jahn, R.; Niemann, H. Proteolysis of Snap-25 by Type-E and Type-a Botulinal Neurotoxins. *J. Biol. Chem.* **1994**, *269*, 1617−1620.
(35) Blasi, J.; Chapman, E. R.; Link, E.; Binz, T.; Yamasaki, S.; De Camilli, P.; Sudhof, T. C.; Niemann, H.; Jahn, R. Botulinum neurotoxin A selectively cleaves the synaptic protein SNAP-25. *Nature* **1993**, *365*, 160−163.
(36) Vaidyanathan, V. V.; Yoshino, K.; Jahnz, M.; Dorries, C.; Bade, S.; Nauenburg, S.; Niemann, H.; Binz, T. Proteolysis of SNAP-25 isoforms by botulinum neurotoxin types A, C, and E: domains and amino acid residues controlling the formation of enzyme-substrate complexes and cleavage. *J. Neurochem.* **1999**, *72*, 327−337.

https://doi.org/10.1021/acssynbio.2c00426
ACS Synth. Biol. 2023, 12, 153−163

(37) Sekar, K.; Gentile, A. M.; Bostick, J. W.; Tyo, K. E. N-Terminal-Based Targeted, Inducible Protein Degradation in *Escherichia coli*. *PLoS One* **2016**, *11*, No. e0149746.
(38) Ganini, D.; Leinisch, F.; Kumar, A.; Jiang, J.; Tokar, E. J.; Malone, C. C.; Petrovich, R. M.; Mason, R. P. Fluorescent proteins such as eGFP lead to catalytic oxidative stress in cells. *Redox Biol.* **2017**, *12*, 462−468.
(39) Pishesha, N.; Ingram, J. R.; Ploegh, H. L. Sortase A: A Model for Transpeptidation and Its Biological Applications. *Annu. Rev. Cell Dev. Biol.* **2018**, *34*, 163−188.
(40) Zhang, S.; Lebreton, F.; Mansfield, M. J.; Miyashita, S. I.; Zhang, J.; Schwartzman, J. A.; Tao, L.; Masuyer, G.; Martinez-Carranza, M.; Stenmark, P.; Gilmore, M. S.; Doxey, A. C.; Dong, M. Identification of a Botulinum Neurotoxin-like Toxin in a Commensal Strain of *Enterococcus faecium*. *Cell Host Microbe* **2018**, *23*, 169−176.
(41) Zhang, S.; Masuyer, G.; Zhang, J.; Shen, Y.; Lundin, D.; Henriksson, L.; Miyashita, S. I.; Martinez-Carranza, M.; Dong, M.; Stenmark, P. Identification and characterization of a novel botulinum neurotoxin. *Nat. Commun.* **2017**, *8*, No. 14130.
(42) Ito, K.; Bian, H. J.; Molina, M.; Han, J.; Magram, J.; Saar, E.; Belunis, C.; Bolin, D. R.; Arceo, R.; Campbell, R.; Falcioni, F.; Vidovic, D.; Hammer, J.; Nagy, Z. A. HLA-DR4-IE chimeric class II transgenic, murine class II-deficient mice are susceptible to experimental allergic encephalomyelitis. *J. Exp. Med.* **1996**, *183*, 2635−2644.
(43) Greenbaum, J.; Sidney, J.; Chung, J.; Brander, C.; Peters, B.; Sette, A. Functional classification of class II human leukocyte antigen (HLA) molecules reveals seven different supertypes and a surprising degree of repertoire sharing across supertypes. *Immunogenetics* **2011**, *63*, 325−335.
(44) Broide, R. S.; Rubino, J.; Nicholson, G. S.; Ardila, M. C.; Brown, M. S.; Aoki, K. R.; Francis, J. The rat Digit Abduction Score (DAS) assay: a physiological model for assessing botulinum neurotoxin-induced skeletal muscle paralysis. *Toxicon* **2013**, *71*, 18−24.
(45) Schellekens, H. The immunogenicity of therapeutic proteins. *Discovery Med.* **2010**, *9*, 560−564.
(46) Lagassé, H. D.; McCormick, Q.; Sauna, Z. E. Secondary failure: immune responses to approved protein therapeutics. *Trends Mol. Med.* **2021**, *27*, 1074−1083.
(47) Krishna, M.; Nadler, S. G. Immunogenicity to Biotherapeutics - The Role of Anti-drug Immune Complexes. *Front. Immunol.* **2016**, *7*, 21.
(48) Dressler, D.; Hallett, M. Immunological aspects of Botox, Dysport and Myobloc/NeuroBloc. *Eur. J. Neurol.* **2006**, *13*, 11−15.
(49) Zinsli, L. V.; Stierlin, N.; Loessner, M. J.; Schmelcher, M. Deimmunization of protein therapeutics - Recent advances in experimental and computational epitope prediction and deletion. *Comput. Struct. Biotechnol. J.* **2021**, *19*, 315−329.
(50) Salvat, R. S.; Verma, D.; Parker, A. S.; Kirsch, J. R.; Brooks, S. A.; Bailey-Kellogg, C.; Griswold, K. E. Computationally optimized deimmunization libraries yield highly mutated enzymes with low immunogenicity and enhanced activity. *Proc. Natl. Acad. Sci. U.S.A.* **2017**, *114*, E5085−E5093.
(51) Zhao, H.; Verma, D.; Li, W.; Choi, Y.; Ndong, C.; Fiering, S. N.; Bailey-Kellogg, C.; Griswold, K. E. Depletion of T cell epitopes in lysostaphin mitigates anti-drug antibody response and enhances antibacterial efficacy in vivo. *Chem. Biol.* **2015**, *22*, 629−639.
(52) Zhao, H.; Brooks, S. A.; Eszterhas, S.; Heim, S.; Li, L.; Xiong, Y. Q.; Fang, Y.; Kirsch, J. R.; Verma, D.; Bailey-Kellogg, C.; Griswold, K. E. Globally deimmunized lysostaphin evades human immune surveillance and enables highly efficacious repeat dosing. *Sci. Adv.* **2020**, *6*, No. eabb9011.
(53) Deitiker, P.; Oshima, M.; Jankovic, J.; Atassi, M. Z. Influences of HLA DRB1, DQA1 and DQB1 on T-cell recognition of epitopes and of larger regions of the botulinum neurotoxin molecule. *Immunol. Lett.* **2017**, *190*, 257−264.
(54) Oshima, M.; Deitiker, P.; Jankovic, J.; Aoki, K. R.; Atassi, M. Z. Submolecular recognition of the C-terminal domain of the heavy chain of botulinum neurotoxin type A by T cells from toxin-treated cervical dystonia patients. *Immunobiology* **2016**, *221*, 568−576.
(55) Oshima, M.; Deitiker, P.; Jankovic, J.; Atassi, M. Z. Submolecular recognition regions of the HN domain of the heavy chain of botulinum neurotoxin type A by T cells from toxin-treated cervical dystonia patients. *J. Neuroimmunol.* **2016**, *300*, 36−46.
(56) Flynn, T. C. Botulinum toxin: examining duration of effect in facial aesthetic applications. *Am. J. Clin. Dermatol.* **2010**, *11*, 183−199.
(57) Parker, A. S.; Choi, Y.; Griswold, K. E.; Bailey-Kellogg, C. Structure-guided deimmunization of therapeutic proteins. *J. Comput. Biol.* **2013**, *20*, 152−165.
(58) Niesen, F. H.; Berglund, H.; Vedadi, M. The use of differential scanning fluorimetry to detect ligand interactions that promote protein stability. *Nat. Protoc.* **2007**, *2*, 2212−2221.
(59) Blum, T. R.; Liu, H.; Packer, M. S.; Xiong, X.; Lee, P. G.; Zhang, S.; Richter, M.; Minasov, G.; Satchell, K. J. F.; Dong, M.; Liu, D. R. Phage-assisted evolution of botulinum neurotoxin proteases with reprogrammed specificity. *Science* **2021**, *371*, 803−810.
(60) Miyashita, S. I.; Zhang, J.; Zhang, S.; Shoemaker, C. B.; Dong, M. Delivery of single-domain antibodies into neurons using a chimeric toxin-based platform is therapeutic in mouse models of botulism. *Sci. Transl. Med.* **2021**, *13*, No. eaaz4197.

https://doi.org/10.1021/acssynbio.2c00426
ACS Synth. Biol. 2023, 12, 153−163